Journal of
Marine Science and Engineering

MDPI

Article

Study on the Methods of Measurement, Optimization and Forecast of Propulsion Shaft Bearing Load of Ships

Rui Li [1], Ji Wang [1,2,3,*], Ziqi Chen [1], Feixiang Wang [1] and Yujun Liu [1,3]

[1] School of Naval Architecture and Ocean Engineering, Dalian University of Technology, Dalian 116024, China
[2] Collaborative Innovation Center for Advanced Ship and Deep-Sea Exploration, Shanghai 200240, China
[3] State Key Laboratory of Structural Analysis for Industrial Equipment, Dalian 116024, China
* Correspondence: wangji@dlut.edu.cn; Tel.: +86-15542681106

Abstract: The qualit12y of shafting alignment is related to the reliability and safety of a ship's operation, and bearing displacement adjustment (BDA) plays a key role in shafting alignment. To solve the problems encountered in ship shafting alignment in the actual construction, this study focused on the investigation of the shafting load measurement system based on the strain gauge method (SGM), used the optimization method based on quadratic programming (QP) to calculate the BDA and adopted algorithms based on the bearing load influence coefficients (BICs) to forecast the load after the adjustment. The experimental work, as well as the measurement, calculation and analysis of several real ships, indicated that the measurement, optimization and forecasting methods of the bearing load of the propulsion shafting of large ships in this study would be significant for guiding the actual construction work of ship shafting alignment.

Keywords: propulsion shafting; bearing load; measurement; optimization; forecast

check for updates

Citation: Li, R.; Wang, J.; Chen, Z.; Wang, F.; Liu, Y. Study on the Methods of Measurement, Optimization and Forecast of Propulsion Shaft Bearing Load of Ships. *J. Mar. Sci. Eng.* **2023**, *11*, 1324. https://doi.org/10.3390/jmse11071324

Academic Editor: Rosemary Norman

Received: 27 May 2023
Revised: 21 June 2023
Accepted: 27 June 2023
Published: 29 June 2023

1. Introduction

Modern transport ships are becoming increasingly high-speed and large-scale ships, requiring the installation of propellers and propulsion shafts with larger diameters to generate greater propulsion, which greatly increases the load on bearings, especially on the after stern tube bearing (STB). Poor shafting alignment of the ship propulsion system will cause rapid wear or even damage to the after STB and may also exacerbate ship hull vibration, seriously affecting the safety and comfort of the ship's operation [1–4]. Therefore, it is particularly essential to ensure good shafting alignment of the ship's propulsion system. Currently, bearing load measurement is generally used to evaluate the quality of the shafting alignment. If the deviation between the actual bearing load and the specified alignment calculation limit exceeds 20% (some regulations require 10%), then the bearing position needs to be adjusted to meet the specification requirements. Therefore, accurate bearing load measurement results can effectively avoid the occurrence of bearing bush burning, incorrect gear meshing, abnormal vibration and other conditions, which are of great significance to ensure the quality of shaft installation [5,6].

The bearing load of a large shaft system cannot often be measured directly but can be calculated through the indirect measurement of other variables. Currently, there are two traditional methods for measuring the bearing load of large shaft systems, namely, the jack-up method and the strain gauge method (SGM) [7–10]. The jack-up method involves installing a jack and a displacement sensor at a specific position next to the shaft bearing to measure the pressure and shaft displacement of the jack at the same time and then draw a jack-up curve to determine the bearing load. However, this method requires a certain amount of working space for appropriate measurement, and thus, it is often hindered in actual engineering by space constraints [11]. However, the SGM can overcome the spatial limitations of the jack-up method. Resistance strain gauges are arranged and pasted on some key cross-sections of the shaft surface, and then the strain values from each strain gauge at different cross-sections are measured and recorded while rotating the shaft, based on which the shaft moment can be calculated. Furthermore, the bearing load can also be calculated by establishing a force and moment equilibrium equation [10,12]. Tupkari [11] provided a theoretical introduction to the jack-up method using a hoisting jack, presented the measuring method, as well as the analysis of its advantages and disadvantages, and finally calculated the bearing load using the jack-up curve. Nasselqvist [13] proposed a resistance-strain-gauge-based method for measuring the load of hydropower units and verified the accuracy of the method through numerical calculations with the measurement results of shaft orbits. Zhang [14] arranged three strain gauges on the shaft to identify the bearing load through a force and moment equilibrium equation, designed the bearing system test rig for verification and discussed the sensitivity of the distribution of strain gauges to the bearing load identification. Keshava [10] used a wireless strain testing system to measure the strain at different points on the shaft section and calculated the change in bearing load caused by bearing displacement using the calculation model established, which, combined with the bearing load in the straight-line alignment condition, led to the actual bearing load. Batra [15] studied the load measurement method based on the SGM to address the problems with the jack-up method in bearing load measurement and developed alignment calculation software to achieve the optimization of shafting alignment. Lee [16] adopted the SGM to conduct an in-depth study on the shafting displacement state under the influence of propeller hydrodynamics. Choi [17] presented a novel approach of inverse analysis using deep reinforcement learning to predict the shaft deformation following stern hull deformation, where the validation was verified using a medium-sized oil/chemical tanker. However, although the methods of shafting static reasonable alignment and measurement are relatively mature, there is still a lack of practical measurement methods for shafting load measurement to evaluate the quality of shafting alignment in operation, which makes it impossible to further guide the optimization of shafting alignment.

In order to ensure a good load distribution of the shafting in operation, a large number of scholars have adopted various methods to optimize their designs of bearing displacement. Yang [18] optimized the design of a single STB of a 50K-DWT petroleum product tanker, in which they comprehensively considered the characteristics of shafting alignment and whirling vibration and provided the optimal solution for adjustment of the axial and vertical displacement of the intermediate bearing. Lai [19] proposed an optimization model that combines weight coefficient optimization with a linear programming algorithm, which adjusts the vertical position of each bearing to simultaneously optimize the alignment quality and vibration characteristics of the motor drive shaft system, shedding new light on the comprehensive optimization of shaft vibration reduction and alignment. Deng [20] proposed a method for fitting the shafting characteristic function by using the GA-BP (genetic algorithm–backpropagation) neural network to achieve shaft alignment optimization, providing guidance for the installation and adjustment of ship shafting. Considering the current deficiencies in ship shafting design, Lai [21] put forward the MDO theory, which determines the KPI of a shafting system design and its optimization weight through questionnaire surveys and gave a new idea for multidisciplinary optimization designs of a shaft system. Liu [22] proposed the invasive weed optimization (IWO) algorithm to optimize the shaft alignment in both directions, with the objective function of minimizing the STB load, which resulted in a significant reduction in the STB load after the optimization of the BDA. Juang [23] used the ARPSO algorithm, together with the three-bending moment equation, to obtain the global optimal design parameters for the bearing offset. Yin [24] used the fireworks algorithm to develop a multidisciplinary optimization model that considers the shafting alignment, whirling vibration and dynamic oil film stiffness.

Batra [15] combined the single-objective linear programming algorithm with the multi-objective linear programming algorithm to calculate the BDA, but the feasibility of his algorithm has not been verified by actual ship operations. Sverko [25] used the genetic algorithm to solve for the optimal displacement of each bearing. However, due to the poor solving efficiency of this large-scale optimization algorithm, it is not applicable for actual on-site operations. The traditional algorithm of BDA is usually based on the optimization methods of linear programming, which focuses only on the optimization of the bearing load. This will easily lead to the calculated displacement value to approach the height boundary value, and the accuracy of the optimization results has not been verified by actual ship operations. Furthermore, there are no efficient and accurate bearing load measurement methods.

To address the above issues, this study proposed a novel method to assess the bearing load under a dynamic running state and designed a large-scale shaft test rig for measurement verification based on the approach of SGM. A QP optimization algorithm for multi-objective functions in shafting alignment was proposed, using "minimum BDA" and "minimum STB load" as the objective functions, with both the weight of the BDA and STB load adjusted during the optimization. To reduce the measurements and effectively shorten the construction cycle for shafting alignment, the load forecast algorithm was also investigated based on BICs. The proposed bearing load measurement, forecast and optimization methods were verified using the shafting system measurement results of five container ships, and thus, these methods are of great guiding significance for the design, installation and inspection of large-scale ship propulsion shafting.

2. Modeling

Figure 1 outlines the flow of the approach adopted in this study. First, with its accuracy verified by a self-designed large-scale shaft test rig, the proposed SGM was applied to the bearing load measurement of actual ships. Second, the modeling of the ship's propulsion shaft system was used for the alignment calculation, and the data obtained were then used to perform the BDA optimization based on a QP algorithm and bearing load forecasting study based on the BIC principle. Finally, the results were analyzed and compared with the measured data from five container ships.

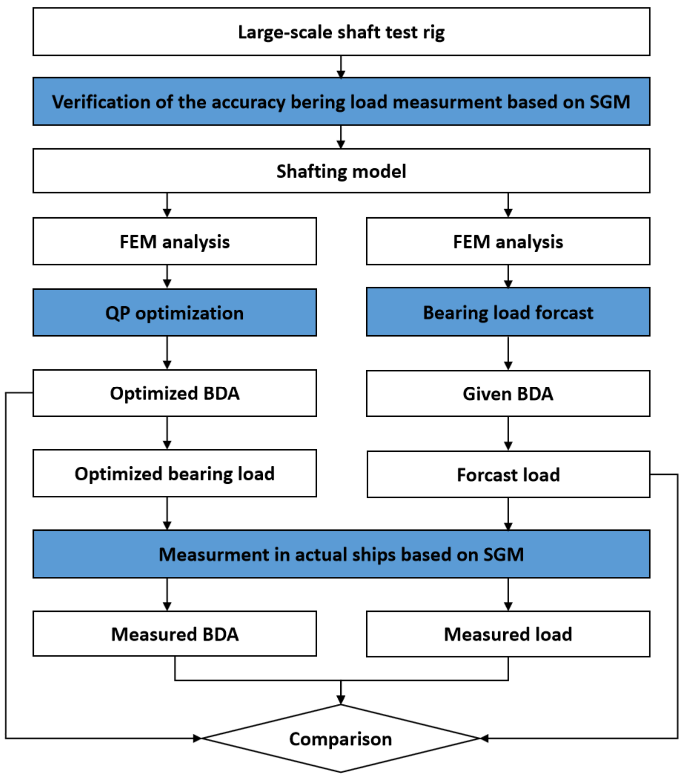

Figure 1. Study outline.

2.1. Bearing Load Measurement Method

This study adopted the measurement principle based on a resistance strain gauge and the half-bridge wiring method in terms of the bridge connection of the strain gauge. As shown in Figure 2, two sets of strain gauges R1 and R2 were pasted on the relative upper and lower surfaces, respectively, of the same cross-section of the tested shaft; A, B, C and D are the wiring joints; UBD is the voltage between B and D. The half-bridge wiring method has the advantages of high precision and mutual temperature compensation [7].

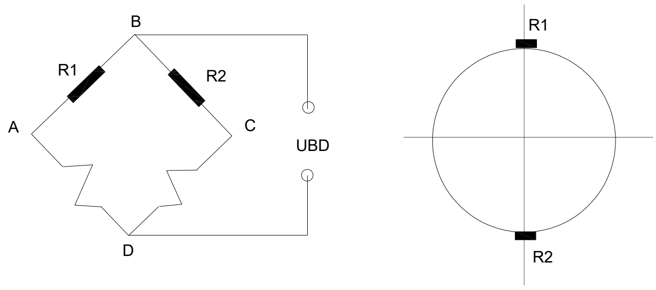

Figure 2. Half-bridge wiring method.

When clinging closely to the surface of the shaft, the strain gauge experiences tensile compression deformation during the rotation of the shaft, the resistance value of which changes accordingly, as shown in the following equation:

$$\frac{\Delta R}{R} = K \times \varepsilon, \quad (1)$$

where R is the initial resistance value, ΔR is the resistance variation, K is the proportional coefficient and ε is the strain.

Suppose the angular velocity of shaft rotation is ω, the measured strain is then a harmonic variation, and the strain frequency is equal to the shaft rotation frequency, as shown in Figure 3:

$$\varepsilon = a \cos \omega t, \quad (2)$$

where ε is the dynamic strain and a is the amplitude of the strain.

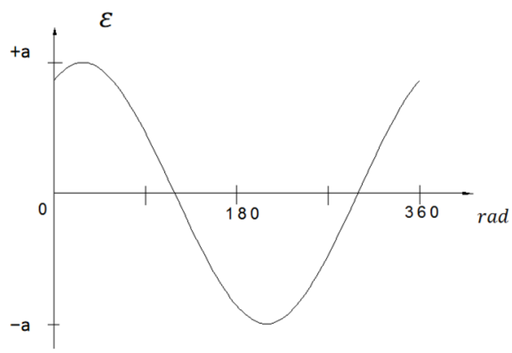

Figure 3. Location distribution of strain gauge measuring points.

The bending moment of the shaft section in a running state is different from that in the static state, and thus, it is necessary to decompose the bending moment at the cross-section along the horizontal and vertical directions, where the horizontal bending moment is M_z and the vertical bending moment is M_x. When the number of harmonics is considered:

$$M_x = \sum_{n=1}^{k} A_n \cos(n\beta + \gamma_{xn}), \quad (3)$$

$$M_z = \sum_{n=1}^{k} B_n \cos(n\beta + \gamma_{zn}), \tag{4}$$

the strain can then be shown as

$$\varepsilon = \sum_{n=1}^{k} a_n \cos\beta \cos(n\beta + \gamma_{xn}) + \sum_{n=1}^{k} b_n \sin\beta \cos(n\beta + \gamma_{zn}), \tag{5}$$

where n is the harmonic order ranging from 1 to k, A_n is the component of the horizontal bending moment in order n, B_n is the component of the vertical bending moment in order n, a_n is the component of horizontal strain in order n, b_n is the component of vertical strain in order n, β is the rotation angle and γ is the phase angle of harmonic order.

In calculating the shaft load, the weight of the tail shaft and propeller shall be corrected according to their actual floating state, and the bending moment of the shaft cross-section shall be calculated with the consideration of such a correction in the actual measurement:

Bending stress:

$$\sigma = \pm Ea\beta_0/C, \tag{6}$$

Bending moment:

$$M = \pm W\sigma \text{ or } M_z = \pm W\sigma\cos\delta,\ M_x = \pm W\sigma\sin\delta, \tag{7}$$

where E is the elastic modulus, W is the flexural section coefficient, C is the bridge coefficient, β_0 is the line correction coefficient and δ is the moment angle.

After the calculation of the bending moment of the shaft section, with the usual division of the shaft into several shaft sections bounded by the measuring points of the strain gauge and the change points of the cross-section, the actual load at the bearing can be solved through an equilibrium equation of force and bending moment. Take the calculation of the vertical load of a single supporting point model shown in Figure 4 as an example. One set of strain gauges is at C, at a distance of x_1 in front of the flange, and the other set is at D, at a distance of x_2 to the rear end of the intermediate bearing. With the two sets of strain gauges, the bending strain at the clinging cross-section is obtained through measuring, and then the cross-section bending moment is obtained. Point O is the STB supporting point, and its distance to A, which is the rear end of the bearing, is x'. The reaction force and position of the supporting point of the tail bearing can be calculated through an equilibrium equation of bending moment and force.

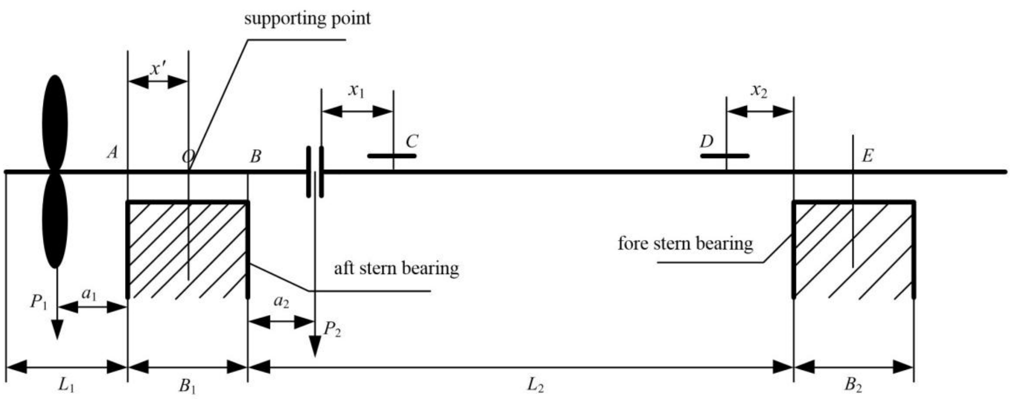

Figure 4. Model of a single supporting point stern shaft.

2.2. Bearing Load Optimization Method

In consideration of the facts that too much BDA should not be performed in an actual situation and the STB requires more attention due to its easy damage caused by complex stress, the double optimization of both the displacement and the STB load should be involved when setting the optimization goal. Since the bearing displacement has positive and negative signs (positive when the bearing position is up and negative when the bearing position is down), the objective function of displacement optimization cannot be constructed through linear programming. Therefore, based on the structural characteristics of the objective function of quadratic programming, this study adopted a QP optimization algorithm to solve the BDA.

QP is one of the optimization algorithms and aims to find the limit value of a quadratic function $Q(x)$ under the constraints of linear equality and linear inequality of variables x_1, $x_2, \ldots, x_\mathrm{n}$ [26]:

$$\begin{gathered} \min Q(\boldsymbol{x}) = \frac{1}{2}\boldsymbol{x}^{\mathrm{T}} H \boldsymbol{x} + \boldsymbol{g}^{\mathrm{T}}\boldsymbol{x}, \\ \text{s.t. } \boldsymbol{a}_i^{\mathrm{T}}\boldsymbol{x} = \boldsymbol{b}_i,\ i = 1, 2, \ldots, m \\ \boldsymbol{a}_i^{\mathrm{T}}\boldsymbol{x} \leq \boldsymbol{b}_i,\ i = m+1, \ldots, p \end{gathered} \tag{8}$$

where $x = (x_1, x_2, \ldots, x_n)$; H is the n-order symmetric matrix; g, a_1, a_2, ... , a_p are n-dimensional vectors; a_1, a_2, ... , a_m are linearly independent; b_1, b_2, ... , b_p are known constants; and $m < n$, $m < p$.

The quadratic term of the quadratic function $Q(x)$ is composed of the square of the independent variable multiplied by its coefficients and then summed, which avoids the mutual cancellation of the bearing displacement due to different signs and realizes the optimization of the displacement. The primary term $g^{\mathrm{T}}x$ is the linear relationship of independent variables; the optimization of the after STB load can be realized by such a relationship because, without the consideration of the support and oil film stiffness, the increase in bearing load caused by displacement is linearly related to displacement. In consideration of the difference between the magnitude of displacement and that of the load, the Heissen matrix (H) is constructed as $\mathrm{diag}_{n\times n}(10^{\lambda}, 10^{\lambda}, \ldots, 10^{\lambda})$, where the consistency of the magnitude of displacement and the adjustment of the displacement proportion during optimization can be achieved through the coefficient λ, and the adjustment of the load proportion during optimization though the addition of coefficient t before the primary term $g^{\mathrm{T}}x$.

(1) Objective function

Based on the above analysis, the objective function was established as follows:

$$\min \boldsymbol{x}^{\mathrm{T}}\boldsymbol{H}\boldsymbol{x} + t\boldsymbol{a}_1^{\mathrm{T}}\boldsymbol{x}, \tag{9}$$

where $x = (\Delta y_1, \Delta y_2, \ldots, \Delta y_i, \ldots, \Delta y_n)$, Δy_i is the BDA of the ith bearing, $H = \mathrm{diag}_{n\times n}(10^{\lambda}, 10^{\lambda}, \ldots, 10^{\lambda})$, λ and t are the influence coefficients that are used to adjust the proportion of displacement and load in the optimization target, $a_i = (a_{1,1}, a_{2,1}, \ldots, a_{i,1}, \ldots, a_{n,1})^{\mathrm{T}}$ and $a_{i,1}$ is the BIC of the ith bearing on the after STB (assuming that bearing #1 is the one after the STB).

(2) Constraints

When the stiffness of the bearing and the oil film is not considered, the load increase caused by the bearing displacement is linearly related to the displacement value, and thus, the load value R_i after the displacement of the ith bearing can be given as

$$R_i = R_{iC} + \sum_{j=1}^{n} a_{j,i}\Delta y_j, \tag{10}$$

where R_{iC} is the measuring load of the ith bearing (C added to subscript) and $a_{j,i}$ is the BIC of the jth bearing on the ith bearing.

Similarly, the bending moment M_i after the displacement of the ith bearing is given as

$$M_i = M_{iC} + \sum_{j=1}^{n} m_{j,i}\Delta y_j, \tag{11}$$

where M_{iC} is the measuring moment of the *i*th bearing (*C* added to the subscript) and $m_{j,i}$ is the bearing moment influence coefficient of the *j*th bearing on the *i*th bearing.

According to the shafting alignment requirements, the bearing load and bending moment shall not exceed a certain range, and thus, the load value R_i and bending moment M_i after the bearing displacement should be within their respective ranges. Therefore, the inequality constraints are set as follows:

$$R_{iD} \le R_i \le R_{iS}, M_{iD} \le M_i \le M_{iS}, \Delta y_{iD} \le \Delta y_i \le \Delta y_{iS}, \tag{12}$$

where R_{iD} and R_{iS} are the lower limit of the load value (D as the subscript) and the upper limit of the load value (S as the subscript), respectively, in the alignment specification; M_{iD} and M_{iS} are the lower limit and upper limit of bending moment value, respectively, in the alignment specification; Δy_{iD} and Δy_{iS} are the lower limit and upper limit of the bearing displacement value, respectively.

Considering that during the actual adjustment of the bearings, the construction personnel cannot adjust the front and rear STB through the bulkhead, the equality constraint should be added for such bearings, the BDA of which cannot be performed:

$$\Delta y_i = 0, \tag{13}$$

2.3. Bearing Load Forecasting Method

Measurement of the bearing load based on either the jack-up method or SGM would consume considerable manpower, material resources and time, and affect the progress of ship construction. Therefore, in actual construction, the forecast of the post-adjustment bearing load based on the current bearing load measured and BDA estimated could significantly reduce the number of bearing load adjustments and measurements. Therefore, this study adopted the BIC principle to predict the bearing load.

The so-called BIC refers to the effect on the load of the remaining bearings when the height of the *j*th bearing in the shafting changes with a unit scale (such as 1 mm) [27]. For example, $a_{j,i}$ indicates the change in the *i*th bearing load caused by the unit displacement of the *j*th bearing. When the stiffness of the bearings and the oil film is not considered, these additional loads are linearly related to the displacement of the bearing, as can be shown in the following equation:

$$R_i = R_{0,i} + a_{1,i}\Delta y_1 + \ldots a_{j,i}\Delta y_j + \ldots + a_{n,i}\Delta y_n, \tag{14}$$

where $R_{0,i}$ represents the load value of the *i*th bearing before the bearing height is adjusted.

The BIC matrix of a shaft system can be constructed in the following form using the three-moment method or finite element method:

$$\boldsymbol{A} = \begin{bmatrix} a_{1,1} & a_{1,2} & \cdot & \cdot & \cdot & a_{1,i} & \cdot & \cdot & \cdot & a_{1,n} \\ a_{2,1} & a_{2,2} & \cdot & \cdot & \cdot & a_{2,i} & \cdot & \cdot & \cdot & a_{2,n} \\ \cdot & \cdot & & & & \cdot & & & & \cdot \\ \cdot & \cdot & & & & \cdot & & & & \cdot \\ \cdot & \cdot & & & & \cdot & & & & \cdot \\ a_{i,1} & a_{i,2} & \cdot & \cdot & \cdot & a_{i,i} & \cdot & \cdot & \cdot & a_{i,n} \\ \cdot & \cdot & & & & \cdot & & & & \cdot \\ \cdot & \cdot & & & & \cdot & & & & \cdot \\ \cdot & \cdot & & & & \cdot & & & & \cdot \\ a_{n,1} & a_{n,2} & \cdot & \cdot & \cdot & a_{n,i} & \cdot & \cdot & \cdot & a_{n,n} \end{bmatrix}_{n\times n}, \tag{15}$$

It should be noted that the bearing reaction force used in the construction of the influence coefficient matrix should only be the force caused by the bearing elevation variation, which is irrelevant given the external load and self-weight. The value of the bearing load after adjusting the bearing displacement can be calculated using the following equation:

$$\boldsymbol{R} = \boldsymbol{R}_0 + \boldsymbol{A}^{\mathrm{T}}\Delta\boldsymbol{Y}, \tag{16}$$

where $R = [R_1\ R_2\ \ldots\ R_i\ \ldots\ R_n]^{\mathrm{T}}$, where Ri is the load value of the ith bearing after the bearing height is adjusted; $R_0 = [R_{0,1}\ R_{0,2}\ \ldots\ R_{0,i}\ \ldots\ R_{0,n}]^{\mathrm{T}}$ is the bearing load measurement matrix; and $\Delta Y = [\Delta y_1\ \Delta y_2\ \ldots\ \Delta y_i\ \ldots\ \Delta y_n]^{\mathrm{T}}$ is the BDA matrix.

3. Results and Discussion

3.1. Measurement of Bearing Load under Dynamic Operating Conditions

3.1.1. Measurement System and Scheme

In order to study the bearing load measurement method in the running state condition of a large-scale shaft, a large-scale shaft test rig was designed and built. The rig consisted of three shaft sections and four bearings. The total length of the shaft was 12.80 m and the weight was 15.35 t. The shaft was driven by a 22 kW motor, with a maximum speed of 250 rpm. The transmitting end of strain data wireless acquisition system adopted was a MicroStrain V-Link-200, and the receiving base station adopted was a LORD MicroStrain WSDA-Base-LXRS, which could realize the remote and rapid acquisition of strain data in a running state condition, with a resolution of ±1 με, an accuracy of ±1% F.S. and a transmission distance of 70 m. Four pressure sensors were equipped under each bearing pedestal, with a resolution of ±0.01 kg and an accuracy of ±1% F.S, as shown in Figure 5, such that the actual load of the bearing could be directly measured and then verified through comparison with the calculated load of the bearing from the measurement.

Figure 5. Large-scale shaft test rig.

The wireless strain transmitter V-Link-200 had four full-bridge nodes, and each node had five ports. For example, the ports of node 1 were SP+, S1+, S1−, GND and S1S; the ports of node 2 were SP+, S2+, S2−, GND and S2S; and the following ports were all named like these. When the strain gauges were pasted, the four strands of wires of the strain gauge were connected in pairs by means of the full-bridge connection, and the wire ends were connected to the corresponding interfaces of the transmitting nodes. In addition, it was necessary that the wireless strain transmitter was firmly fixed on the shaft, as shown in Figure 6. The wireless acquisition base station was connected to the computer.

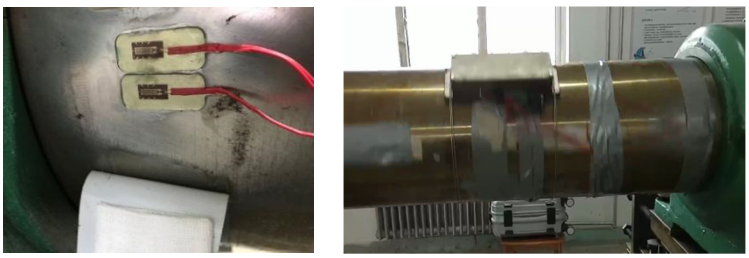

Figure 6. Strain gauge pasting and wireless remote control acquisition equipment.

The installation of the angle measuring device could be performed by means of coordinate paper. First, the induction magnet was placed directly vertically above the shaft, in the same line as the strain gauge. Then, the angle sensor was installed on the horizontal support, the height of which was adjusted to align the sensor with the coordinate paper at a 90° angle, as shown in Figure 7.

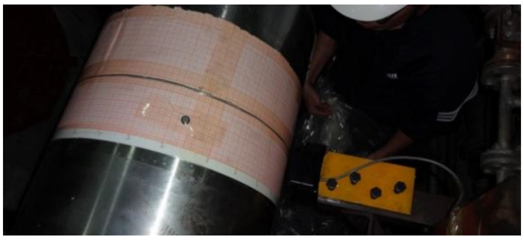

Figure 7. Installation of the angle-measuring equipment.

Before the data acquisition, the shaft was rotated via manual control so that the strain gauge and the induction magnet were aligned to the angle measurement sensor, and the position of the strain gauge was then considered as the initial position. After that, the wireless strain transmitter was activated using the remote control switch. During data acquisition, the motor and angle acquisition equipment were started at the same time so that the strain data and the corresponding angle were synchronously recorded.

The verification of the reliability of the bearing load measurement method in a running state condition was carried out using the large-scale bearing system test rig shown in Figure 4. There was a total of four bearings in the bearing system test rig, which were numbered bearing no. 1, bearing no. 2, bearing no. 3 and bearing no. 4 going from the tail end to the motor end. Pressure sensors were installed under each bearing to measure the load data for reference.

3.1.2. Measurement Results Comparison

The pressure sensor measurement method and the SGM were used to measure the loads of each bearing at different rotational speeds to verify the accuracy of the SGM. The comparison of bearing loads under the same working conditions was shown in Table 1.

Table 1. Comparison of the bearing load measurement results based on the pressure sensors and SGM at different rotational speeds.

Bearing Load (kN)	20.5 (rpm)			42.6 (rpm)		
	Pressure Sensor	Strain Gauge	Relative Error	Pressure Sensor	Strain Gauge	Relative Error
Bearing no. 1	4276	4135	3.30%	4088	3965	3.01%
Bearing no. 2	195	226	15.90%	369	393	6.50%
Bearing no. 3	1512	1444	4.50%	1455	1461	0.41%
Bearing no. 4	1816	1745	3.91%	1822	1693	7.08%
	67.4 (rpm)			119.6 (rpm)		
Bearing no. 1	4111	4063	1.17%	4118	3992	3.06%
Bearing no. 2	366	351	4.10%	365	422	15.62%
Bearing no. 3	1456	1422	2.34%	1475	1510	2.37%
Bearing no. 4	1820	1650	9.34%	1805	1546	14.35%

Table 1 illustrates the comparison of the bearing load measurement results at four different speeds: 20.5, 42.6, 67.4 and 119.6 rpm. It can be seen that the results based on the SGM were very close to the direct measurement results of the pressure sensor. The maximum relative errors for the four bearings were 3.30%, 15.90%, 4.50% and 14.35%, respectively, while the minimum relative errors were 1.17%, 4.10%, 0.41% and 3.91%, respectively. The

SGM had a higher accuracy with a larger bearing load. The errors for bearings no. 2 and no. 4 were larger, and the possible reasons were as follows: the structural parameters of the shaft system were appropriately simplified during the numerical calculation, which may have caused errors. The equivalent supporting point position of the bearing, assumed to be the mid-section of the bearing, was different from that in curved state. Because of the limited shaft structure arrangement, the strain gauges on both sides of bearings no. 2 and no. 4 were relatively close to each other, which caused a larger error. Overall, the bearing load measurement based on the SGM can meet the requirements of a shaft system in a dynamic condition.

3.2. Bearing Displacement Adjustment and Optimization

The calculation and analysis were carried out using the examples of three container ships manufactured by a large shipyard in China to verify the feasibility of using the QP algorithm with the BDA data. The relevant details were as follows: First, the measurement data, including the measured load data of each bearing after the shaft system was installed, the actual BDA (the final BDA obtained through repeated adjustment based on the actual construction experience) and the measured bearing load data (by SGM) after adjustment during the on-site construction process were all recorded. Second, the actual measured load after the bearing adjustment was taken as the target load for the theoretical calculation (the target load could be set by the upper and lower limits of the load constraint), and then by setting the corresponding equality constraint based on the unadjusted bearings, the theoretically calculated BDA using the QP algorithm described above was obtained. Finally, the theoretically calculated amount and the actual BDA during the construction process were compared to verify the accuracy of the method.

The specification of a ship and shaft system of 12,500 TEU is listed in Table 2. Table 3 shows the measured data and the theoretically calculated BDA of the 12,500 TEU#1 container ship. The ship contained four intermediate bearings (IBs), of which only IB2 and IB3 were actually adjusted for displacement. It could be seen from Table 1 that IB2 and IB3 were both adjusted upward, and the actual BDA values were 0.7 mm and 0.8 mm, respectively, resulting in a decrease in the load of the front bearing (Fwd) of the stern tube bearing (STB) and an increase in the load of IB3 and that of IB4 after adjustment. The theoretical calculation revealed that the displacement adjustment of IB2 was consistent with the actual measured value. However, it can be seen that a deviation occurred between the BDA measured value and the calculated value of IB3. This deviation from the actual shaft system was due to the fact that the structural parameters of the shaft system were simplified models in the calculation, and some shaft sections with special structures were processed as others. In addition, the deviation could have also been caused by an unreasonable distribution position of the strain gauges in the complex site environment. It should be noticed that the reading error by the shipyard workers during the measurement, as well as the yard dock condition and sea states during the measurement, might have also influenced the results and caused deviations to some extent.

Table 2. Specification of ship and shaft system of 12,500 TEU.

Parameter	Value
L × B × D (m)	350 × 51.2 × 29.1
Main engine	59,800 kW × 84 rpm
Shaft system	Materials: forged steel (50 Mn-C)
	Propeller shaft (L × D): 14,375 mm × 985 mm
	Intermediate shaft (L × D): (13,875, 14,255, 13,150) × 825 mm

Table 3. Comparison of the BDA values calculated using the QP algorithm with the actual measurements (12,500 TEU#1).

		Load (t)		Adjustment of Bearing Displacement (mm)	
		Before	After (Target)	Actual Value	Calculation
STB	Fwd	39.80	32.15	/	/
IB	#1	24.04	/	/	/
	#2	33.78	/	0.7	0.7
	#3	30.30	31.73	0.8	0.74
	#4	24.02	29.29	/	/
MB	MEA	30.80	/	/	/

For Tables in this study, the following explanations are necessary: load direction—downward as positive; signs for bearing displacement adjustment—positive for upward adjustment of the bearing and negative for downward adjustment. The intermediate bearings in the table are numbered from stern to bow.

The specifications of the ship and shaft system of 4250 TEU are listed in Table 4. Table 5 shows the measured data and the theoretically calculated BDA of the 4250 TEU container ship, which contained only one intermediate bearing; it was lowered by 1.2 mm during the actual adjustment. Considering that other bearings were not adjusted, the BDA values of other bearings were set to zero, except for IB1 during the theoretical calculation. The theoretical calculation showed that the downward adjustment of IB1 was 1.1 mm, which was close to the measured value.

Table 4. Specification of the ship and shaft system of 4250 TEU.

Parameter	Value
L × B × D (m)	235 × 41.2 × 20.1
Main engine	23,420 kW × 84 rpm
Shaft system	Materials: forged steel (40 Mn)
	Propeller shaft (L × D): 11,670 mm × 750 mm
	Intermediate shaft (L × D): (8870, 3545, 3115) × 620 mm

Table 5. Comparison of the BDA values calculated using the QP algorithm with the actual measurements (4250 TEU).

		Load (t)		Adjustment of Bearing Displacement (mm)	
		Before	After (Target)	Actual Value	Calculation
STB	Fwd	8.92	13.70	/	/
IB	#1	49.71	44.72	−1.2	−1.1
MB	MEA	/	/	/	/
	MEF	/	/	/	/

The specifications of the ship and shaft system of 6600 TEU are listed in Table 6. Table 7 shows the measured data and the theoretically calculated BDA of a 6600 TEU container ship, which contained three intermediate bearings, but only IB2 and IB3 had their bearing heights adjusted, resulting in an increase in the load of the front STB, IB1 and IB2, and a decrease in the load of IB3 after the adjustment. The theoretical calculation revealed that both IB2 and IB3 were adjusted downward, and the calculated value was close to the actual measured adjustment value.

Table 6. Specification of the ship and shaft system of 6600 TEU.

Parameter	Value
L × B × D (m)	282 × 35.25 × 20.3
Main engine	29,820 kW × 104 rpm
Shaft system	Materials: forged steel (40 Mn-C)
	Propeller shaft (L × D): 13,045 mm × 770 mm
	Intermediate shaft (L × D): (13,450, 12,189) × 770 mm

Table 7. Comparison of the BDA values calculated using the QP algorithm with the actual measurements (6600 TEU).

		Load (t)		Adjustment of Bearing Displacement (mm)	
		Before	After (Target)	Actual Value	Calculation
STB	Fwd	13.37	16.60	/	/
IB	#1	21.52	21.85	/	/
	#2	17.52	19.23	−0.5	−0.7
	#3	19.02	15.63	−0.7	−0.9
MB	MEA	/	/	/	/

3.3. Bearing Load Forecast

Take a 12,500 TEU series container ship manufactured in a shipyard in China as an example. First, the load value was measured before the bearing adjustment; then, the bearings were adjusted up or down for a certain amount in height, and then the load value of the bearings was measured; finally, the adjusted load value that was calculated using the theoretical method with the above-mentioned equation was compared with the measured load value.

Table 8 shows the measured data of a 12,500 TEU#2 container ship and the theoretically calculated bearing load value after the bearing displacement. IB2, IB3 and IB4 were reduced by 0.17 mm, 0.15 mm and 0.11 mm, respectively. As shown in the table, the relative error between the theoretically calculated value and the measured value of the three intermediate bearing loads was around 4%.

Table 8. Comparison of the bearing load calculated by the given BDA with the actual measurements (12,500 TEU#2).

		Load (t)	Bearing Displacement Adjustment (mm)	Load (t)		Relative Error (%)
		Before		After	Calculation	
STB	Fwd	27.05	/	/	/	/
IB	#1	/	/	/	/	/
	#2	40.60	−0.17	36.44	38.08	4.50
	#3	35.42	−0.15	34.39	35.63	3.61
	#4	30.23	−0.11	31.97	30.68	4.04
MB	MEA	/	/	/	/	/

Table 9 shows the measured data and the theoretically calculated bearing load of a 12,500 TEU#3 container ship after a bearing displacement. The ship had two intermediate bearings adjusted upward, and the relative error between the theoretically calculated value and the measured value of the bearing load after the bearing displacement shown in the table was within 4%.

Table 9. Comparison of the bearing load calculated using the given BDA with the actual measurements (12,500 TEU#3).

		Load (t)	Bearing Displacement Adjustment (mm)	Load (t)		Relative Error (%)
		Before		After	Calculation	
STB	Fwd	39.38	/	32.43	33.22	2.44
IB	#1	24.19	/	/	/	/
	#2	33.41	0.7	/	/	/
	#3	30.31	0.8	32.35	31.54	2.50
	#4	24.24	/	28.79	27.77	3.54
MB	MEA	30.61	/	/	/	/

4. Conclusions

This study proposed a novel method to assess the bearing load in a dynamic running state and designed a large-scale shaft test rig for measurement verification. The feasibility of this study regarding the bearing load optimization and forecasting methods was verified using the measured data of five container ships. The main conclusions drawn were as follows:

(1) With the application of the large-scale shaft test rig, the maximum error of the bearing load measurement based on the SGM under different speeds was 15.90%, while the minimum error was 0.41%. The SGM had higher accuracy with a larger bearing load, which laid a foundation for the study of bearing load variation regularity in a dynamic running state.

(2) It was reasonable and feasible to use the QP algorithm to guide the optimization of bearing displacement of an actual ship shaft system. The BDA measurement results of three different container ships showed that the maximum relative error was 40%, but the deviation value was within ± 0.2 mm, indicating a higher accuracy. Therefore, the QP algorithm could provide good guidance for the ship designers and construction units in shafting alignment work.

(3) The bearing load measurement results of two container ships indicated that the maximum error of the method of forecasting the bearing load based on the BIC principle was 4.50%, which demonstrated that the BIC method was effective at reducing the construction cycle of the shafting alignment work.

(4) The relative deviation between the measured and analyzed values was presumed to be due to the influence of simplified shafting modeling errors, strain gauge distribution locations and measurement errors of the shipyard workers. Therefore, further investigation will be needed to determine the cause of the deviation and solve the problem.

The approach proposed in this study is of great guiding significance for the design, installation and inspection of propulsion shafting systems for large ships.

Author Contributions: Conceptualization, R.L. and J.W.; methodology, R.L. and Y.L.; validation, J.W.; software, Z.C.; formal analysis, R.L.; data curation, J.W.; writing—original draft preparation, F.W.; writing—review and editing, Z.C.; supervision, R.L., J.W. and Y.L. All authors have read and agreed to the published version of the manuscript.

Funding: This research was funded by the Dalian Science and Technology Innovation Fund Dual Key Program (No. 2018J11CY004) and the Dalian Science and Technology Innovation Fund Program (No. 2019J12GX024).

Institutional Review Board Statement: Not applicable.

Informed Consent Statement: Not applicable.

Data Availability Statement: The data are available on request.

Acknowledgments: The authors would like to express their gratitude to Dalian Science and Technology Innovation Fund and relevant shipyards units.

Conflicts of Interest: The authors declare no conflict of interest.

Nomenclature

BDA	Bearing displacement adjustment
QP	Quadratic programming
SGM	Strain gauge method
BIC	Bearing load influence coefficients
STB	Stern tube bearing
IB	Intermediate bearings
MB	Main engine bearings
Fwd	Forward
MEA	Main engine after
MEF	Main engine forward

References

1. Lei, J.; Zhou, R.; Chen, H.; Gao, Y.; Lai, G. Experimental investigation of effects of ship propulsion shafting alignment on shafting whirling and bearing vibrations. *J. Mar. Sci. Technol.* **2022**, *27*, 151–162. [CrossRef]
2. Litwin, W. Water-lubricated bearings of ship propeller shafts—Problems, experimental tests and theoretical investigations. *Pol. Marit. Res.* **2009**, *16*, 4. [CrossRef]
3. Litwin, W.; Dymarski, C. Experimental research on water-lubricated marine stern tube bearings in conditions of improper lubrication and cooling causing rapid bush wear. *Tribol. Int.* **2016**, *95*, 7. [CrossRef]
4. Zhang, S.; Long, Z.; Yang, X. Reaction force of ship stern bearing in hull large deformation based on stochastic theory. *Int. J. Nav. Arch. Ocean Eng.* **2020**, *12*, 10. [CrossRef]
5. Vizentin, G.; Vukelic, G.; Murawski, L.; Recho, N.; Orovic, J. Marine propulsion system failures—A review. *J. Mar. Sci. Eng.* **2020**, *8*, 662. [CrossRef]
6. Yang, H.; Li, J.; Li, X. Calculation of the dynamic characteristics of ship's aft stern tube bearing considering journal deflection. *Pol. Marit. Res.* **2020**, *27*, 107–115. [CrossRef]
7. Zhang, W.; Yang, J.; Li, C.; Dai, R.; Yang, A. Theoretical and experimental research on turbo-generator shaft alignment using strain gauge method. *J. Vib. Control.* **2017**, *23*, 1183–1192. [CrossRef]
8. Vuong, Q.D.; Lee, J.W.; Lee, W.J.; Choi, H.; Seo, K.; Kim, Y.; Jeong, J.H.; Song, M.H.; Lee, J.U. Establishing the true dynamic bending moment of propeller shaft using a single bridge of strain gauge. *Appl. Sci.* **2022**, *12*, 9235. [CrossRef]
9. Wang, Y.; Mohammed, A.; Sarma, N.; Djurovic, S. Double fed induction generator shaft misalignment monitoring by FBG frame strain sensing. *IEEE Sens. J.* **2020**, *20*, 11. [CrossRef]
10. Rao, M.N.; Dharaneepathy, M.V.; Gomathinayagam, S. Computer-aided alignment of ship propulsion shafts by strain-gauge methods. *Mar. Technol. SNAME News* **1991**, *28*, 84–90. [CrossRef]
11. Tupkari, P.D.; Sharma, P.K. Shaft alignment in ship. *Int. J. Adv. Technol. Eng. Sci.* **2014**, *02*, 325–331.
12. Murawski, L. Shaft line alignment analysis taking ship construction flexibility and deformations into consideration. *Mar. Struct.* **2005**, *18*, 62–84. [CrossRef]
13. Nässelqvist, M.; Gustavsson, R.; Aidanpää, J.O. Bearing load measurement in a hydropower unit using strain gauges installed inside pivot pin. *Exp. Mech.* **2012**, *52*, 361–369. [CrossRef]
14. Zhang, S.; Yang, J.; Li, Y.; Li, J. Identification of bearing load by three section strain gauge method: Theoretical and experimental research. *Measurement* **2013**, *46*, 3968–3975. [CrossRef]
15. Batra, A.; Shankar, K.; Swarnamani, S. Propulsion shaft alignment measurements on warships afloat and alignment solution using multi-objective optimization. *J. Mar. Eng. Technol.* **2007**, *6*, 39–49. [CrossRef]
16. Lee, J. Application of strain gauge method for investigating influence of ship shaft movement by hydrodynamic propeller forces on shaft alignment. *Measurement* **2018**, *121*, 261–275. [CrossRef]
17. Choi, S.; Lee, J.; Park, J. Application of deep reinforcement learning to predict shaft deformation considering hull deformation of medium-sized oil/chemical tanker. *J. Mar. Sci. Eng.* **2021**, *9*, 767. [CrossRef]
18. Kim, Y.; Kim, U. Design and analysis of the propulsion shafting system in a ship with single stern tube bearing. *J. Mar. Sci. Technol.* **2020**, *25*, 536–548. [CrossRef]
19. Lai, G.; Liu, J.; Liu, S.; Zeng, F.; Zhou, R.; Lei, J. Comprehensive optimization for the alignment quality and whirling vibration damping of a motor drive shafting. *Ocean Eng.* **2018**, *157*, 26–34. [CrossRef]
20. Deng, Y.; Yang, X.; Huang, Y.; Pan, T.; Zhu, H. Calculation method of intermediate bearing displacement value for multisupported shafting based on neural network. *J. Ship Res.* **2020**, *65*, 286–292.
21. Lai, G.; Lei, J.; Liu, J.; Cao, S.; Qin, H.; Zeng, F.; Zhou, R. Numerical and experimental study on comprehensive optimization for the kpis of ship propulsion shafting design based on mdo. *Ocean Eng.* **2021**, *222*, 108624. [CrossRef]
22. Liu, J.; Lai, G.; Jiang, Z.; Lai, G. Research on the effects of different shafting alignment conditions on the shafting whirling vibration. *J. Ship Mech.* **2022**, *26*, 264–273.

23. Juang, S.H.; Chang, M.; Huang, J. Applying the ARPSO algorithm to shafting alignment optimization design. *Brodogradnja* **2012**, *63*, 13.
24. Yin, H.; Liu, J.; Zeng, F. Coupling characteristic analysis of ship shafting design parameters and research on multidisciplinary design optimization. *J. Vibroeng.* **2020**, *22*, 48–66. [CrossRef]
25. Šverko, D. Shaft alignment optimization. In Proceedings of the 17th Symposium on Theory and Practice of Shipbuilding, Opatija, Croatia, 19–21 October 2006.
26. Sun, Q.; Li, W.; Li, R.; Peng, D.; Guo, Q.; Zhao, Y.; Yue, Q.; Zhong, W. Anchor chain optimization design of a catenary anchor leg mooring system based on adaptive sampling. *J. Mar. Sci. Eng.* **2022**, *10*, 1739. [CrossRef]
27. Zhou, J.L.; Zou, H.J. *Principles and Applications of Ship Shafting Alignment*; People's Communications Publishing House: Beijing, China, 1985; pp. 233–235.